Progress In Electromagnetics Research C, Vol. 115, 111–126, 2021

Design of MIMO/Smart Antenna Arrays Using Different Array Modules for Handheld Device

Panpan Wei* and Wen Geyi

Abstract—In this paper, an eight-element MIMO smart antenna system consisting of two different array modules for handheld device is proposed. The first module is a six-element array operating in N78 (3.3–3.8 GHz) band for 5G, which achieves MIMO functions for receiving and beam scanning for transmitting. The second module is a two-element antenna array, which operates in LTE/WWAN/N78 (0.7–0.91 GHz, 1.63–2.61 GHz, 3.3–3.8 GHz) bands. To take full advantage of the existing antenna resources in the mobile device, the six elements in the first module are combined with the two elements in the second module to form an 8-element array in the overlapping N78 band. Good isolations and envelope correlation coefficients are achieved in the receiving mode by loading L-shaped slots for the combined module. The distribution of excitations for the combined array in the transmitting mode is optimized by the method of maximum power transmission efficiency to direct the beam to the desired direction with maximum possible gain and is realized by an in-house designed beamforming controller. The impacts of the environments on the antenna array performance are investigated.

1. INTRODUCTION

Massive MIMO systems in the future mobile device are required to be integrated with 2G/3G/4G and 5G band antennas with different structures in a limited internal space, which raises a challenge to antenna engineers [1]. There have been reports on the design of multi-frequency band antennas, which integrate multiple antenna structures in one space [2–11]. In [3], an integrated design with MIMO antenna systems for 4G and 5G applications is proposed. The design contains a two-element slot-based MIMO antenna system for 4G and a connected antenna array-based two-element MIMO antenna system for a potential 5G band. A proof-of-concept solution for co-designed millimeter-wave and LTE antennas in a metal-rimmed handset is introduced in [5]. The design shows that the two different antennas can be accommodated in a shared volume and integrated into the same structure, in which the mm-wave antenna does not hinder the low-band performance. However, the two antenna modules of the above mentioned designs do not share the antenna elements of each other. A dual-polarized hybrid 8-element array for 5G application in the smartphone is presented in [6]. The proposed hybrid antenna array is composed of two different 4-element arrays and can achieve MIMO performance in the 2.6 GHz band (2550–2650 MHz). A compact building block composed of a slot antenna and a loop antenna is studied in [7], where the slot antenna and loop antenna share a rectangular clearance, which improves the compactness of the building block. Four such building blocks are used to implement a compact 8-port MIMO array operating in 3.5 GHz band (3.4–3.6 GHz) for 5G metal-rimmed smartphone applications.

As a typical application of multi-antenna technology, beamforming technology has been widely considered in 5G communication research [12–14]. By controlling the excitation of the transmitting antenna elements, beamforming technology can direct the electromagnetic field energy in the desired direction, thus improving the spectrum efficiency, achieving better signal coverage and higher antenna

Received 20 July 2021, Accepted 1 September 2021, Scheduled 10 September 2021
* Corresponding author: Panpan Wei (wpp19850062581@163.com).
The authors are with the Nanjing University of Information Science and Technology, Nanjing 210044, China.

gain. Several beamforming structures have been reported in [15–20]. An 8-element MIMO antenna array operating in GSM1900 (1.88–1.92 GHz) and LTE2300 (2.3–2.4 GHz) bands is proposed for handheld devices in [19]. The antenna array consists of eight planar inverted-F elements printed on an FR4 substrate, exhibiting good beam directivity at different scanning angles. In [20], a millimeter-wave end-fire 5G beam steerable array and a low-frequency antenna are integrated in a mobile terminal. The low frequency antenna can be transparent by using some grating strips between the low frequency antenna and high frequency antenna. The working frequency of millimeter-wave antenna is 22–31 GHz, and the array can scan ± 50 degrees with end-fire radiation, which leads to a good coverage.

The above beam scanning arrays are all composed of identical elements. For the purpose of leveraging the existing antenna assets, the antenna array design using different antenna elements to realize the function of MIMO and beamforming simultaneously is a useful solution but rarely reported. Due to the limitation of space in handheld devices, there will inevitably be strong mutual coupling between antenna elements. How to combine different antenna modules in a compact space to realize MIMO and beamforming technology simultaneously is still a challenge. In an attempt to address the above challenge, this paper proposes a novel design and combines a 2-element planar antenna array module operating in LTE/WWAN/N78 bands with a 6-element inverted-F antenna array module operating in N78 band for 5G, to form a larger 8-element array integrated in a handheld device. In the overlapping N78 band, the combined 8-element array functions as a MIMO system when it is in the receiving mode and as a smart antenna system when it is in the transmitting mode. The configuration of combined array is first optimized to insure that the MIMO performance is achieved. The method of maximum power transmission efficiency (MMPTE) [21, 22] is then used to optimize the distribution of excitations for the combined array to achieve beam steering in the N78 band with the highest possible gain. The optimized distribution of excitations is realized through an in-house-developed digital beamforming controller. A prototype antenna array is fabricated and measured, and both the simulated and measured results meet the performance requirements for the MIMO and the beam steering functions

2. DESIGN OF ARRAY MODULES

2.1. Design of Antenna Elements

Figure 1 shows the detailed dimensions of the two antenna elements respectively for the two different antenna array modules. The antenna elements are built on an FR4 (dielectric constant 4.4, loss tangent 0.02) substrate with the size of 149 mm × 76 mm × 1 mm. The combined 8-element antenna array is composed of two array modules. The first array module consists of six identical folded cubic inverted-F antennas, which are evenly placed on the two long edges of the substrate, as illustrated in Fig. 4. The element is etched on a 5 mm × 5 mm × 3 mm FR4 substrate surface, and its detailed dimensions are shown in Fig. 1(a). The element has two branches to generate two resonances to cover the N78

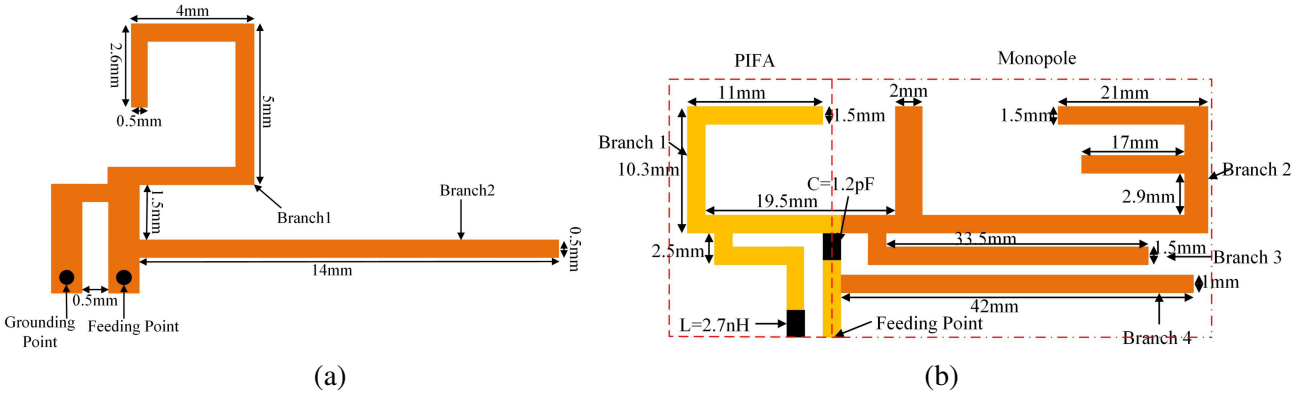

Figure 1. (a) Antenna element of the first module. (b) Antenna element of the second module.

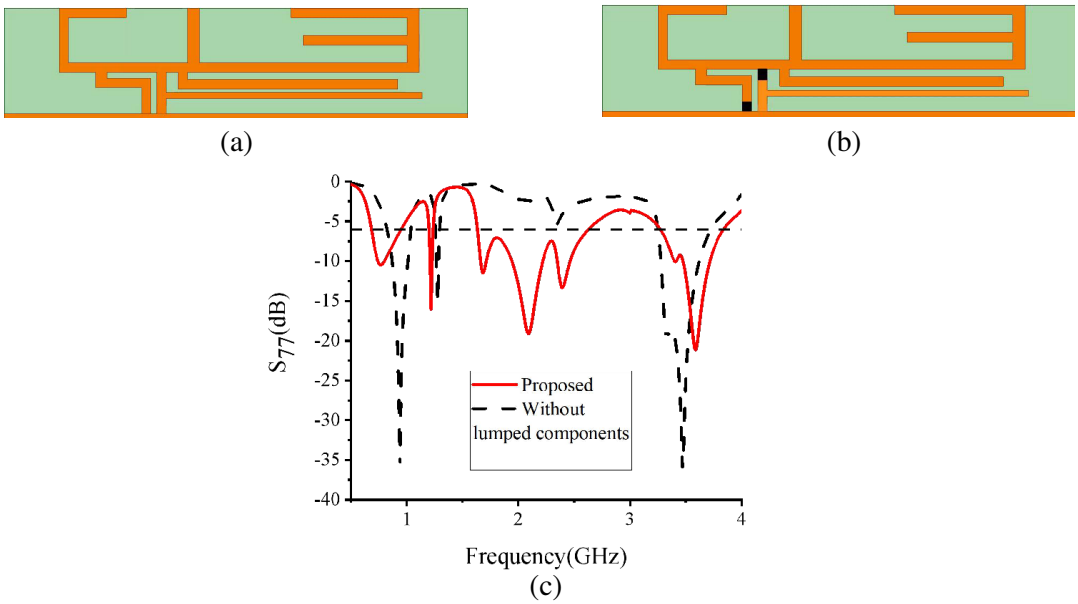

Figure 2. (a) Antenna without lumped components. (b) Proposed antenna. (c) S-parameters with and without inductor and capacitor.

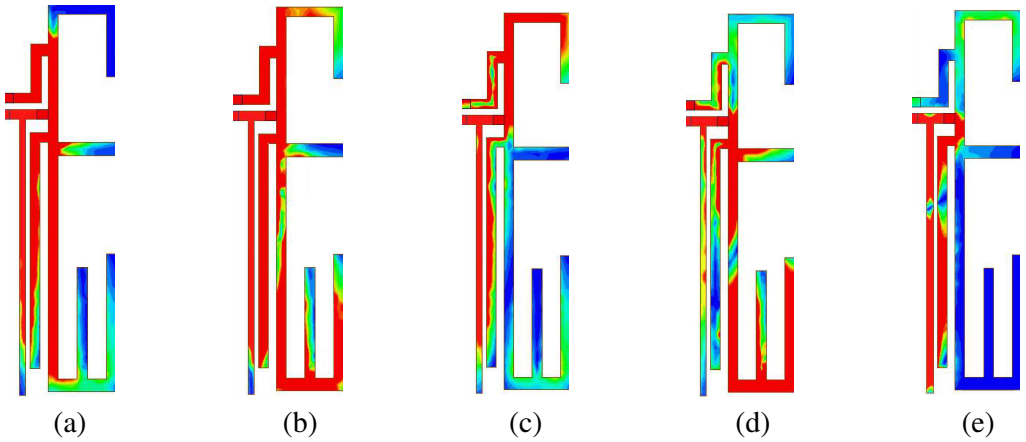

Figure 3. Surface current distributions at resonant frequencies. (a) 0.7 GHz, (b) 1.7 GHz, (c) 2.1 GHz, (d) 2.4 GHz, (e) 3.45 GHz.

band. The high resonant frequency is mainly controlled by branch 1, and the low resonant frequency is mainly controlled by branch 2. The resonant frequency is controlled by adjusting the length of the two branches. In order to increase antenna bandwidth and improve antenna matching, the ground of substrate is partially removed, as shown in Fig. 4(b).

The second module consists of two identical planar antenna elements, which are placed at the top and bottom of the substrate, on the same side as the ground of the substrate. As shown in Fig. 1(b), the antenna element is composed of a planar inverted-F antenna and a monopole antenna with two embedded lumped components, operating in the LTE/ WWAN/N78 (0.7–0.91 GHz, 1.63–2.61 GHz, 3.3–3.8 GHz) frequency bands. The dimensions of the antenna are $59.5 \times 17\,\text{mm}^2$. The lumped capacitor is added to the feeding strip, and the inductor L is connected to the shorting point. After optimization, the values of the two embedded lumped components are set as $C = 1.2\,\text{pF}$ and $L = 2.7\,\text{nH}$. Fig. 2 shows how the capacitor C and inductor L change the lower resonant frequency and improve the match at middle resonant frequency. The surface currents at resonant frequencies are depicted in Fig. 3. As shown in

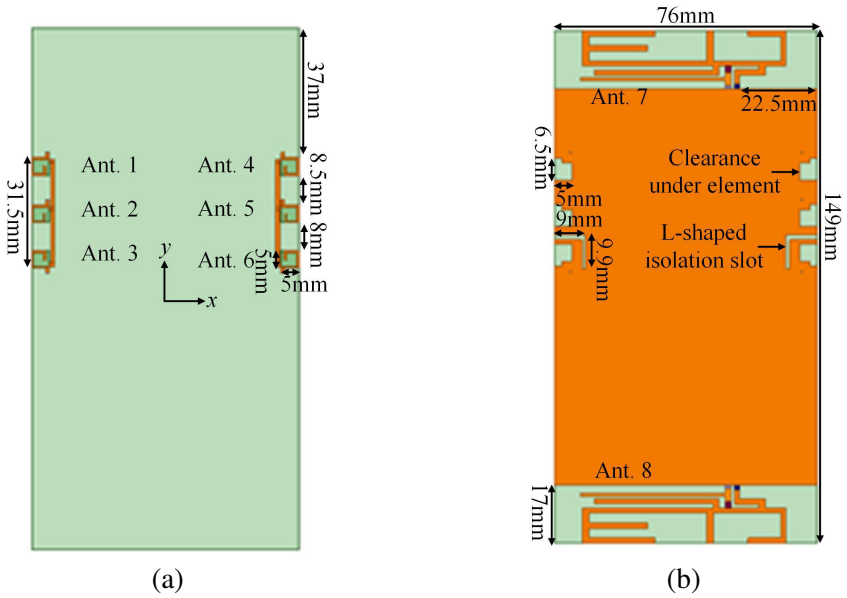

Figure 4. (a) Front view of antenna array. (b) Back view of antenna array.

Figs. 3(a) and (b), the resonances at 0.7 GHz and 1.7 GHz are controlled by the combination of the all the branches. Fig. 3(c) shows that the resonance at 2.1 GHz is mainly generated by the PIFA (branch 1). Fig. 3(d) indicates that the E-shaped monopole (branch 2) generates the resonance at 2.4 GHz. Fig. 3(e) shows that the resonance at 3.45 GHz is generated by the combination of the branch 3 and branch 4.

2.2. Antenna Array Design and MIMO Performance

Figure 4 shows the front and back views of the antenna array. The first module (antenna elements 1–6) is symmetrically placed on the two long edges of the substrate, and the second module (antenna elements 7 and 8) is placed on the top and bottom of the substrate. Since the proposed antenna array is symmetric, only the simulated and measured results of antenna elements 1, 2, 3, and 7 will be depicted. Due to the compact arrangement of elements 1, 2, and 3, with a total length of only 31.5 mm, the isolations among antenna elements do not meet the design requirements. In order to enhance the isolation between the elements, an L-shaped isolation slot is introduced between elements 2 and 3. Fig. 5 shows how the L-shaped slot improves the isolations. In fact, the coupling between elements 2 and 3 is mainly caused by the conduction current on the ground, and therefore a high isolation can be achieved by introducing a slot on the ground.

After the isolation slot is loaded, the S-parameters of elements are shown in Fig. 6 (labeled as Ref_1), and the bandwidths of elements 2 and 3 do not meet the design requirements. We now use a microstrip line to connect the grounding points of elements 1, 2, and 3 to make the three elements electrically connected and therefore electrically larger. As a result, the bandwidth of each element is significantly improved as shown in Fig. 6 (labeled as Proposed). The simulated and measured S-parameters of antenna elements are shown in Fig. 7. The mutual couplings between antenna elements are shown in Fig. 8(a) and are all lower than -10 dB in the operating frequency bands.

The envelope correlation coefficient (ECC) is an important performance index for MIMO system. It can be seen from Fig. 8(b) that the ECCs of the MIMO antenna system are less than 0.1, while the ECCs in MIMO system are generally required to be less than 0.5. As shown in Fig. 8(c), the simulated total efficiency in the operating frequency bands is more than 50%. The measured and simulated gain patterns for the antenna elements 1, 2, 3, and 7 at 3.45 GHz are shown in Fig. 9. All radiation patterns were measured in a microwave anechoic chamber. It can be seen that most element patterns tend to be omnidirectional, and the maximum gain is less than 0 dBi. To enhance the antenna gain and improve

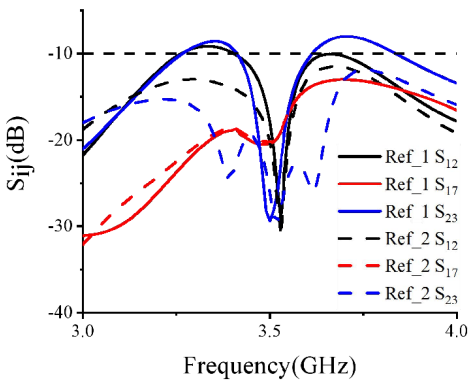

Figure 5. Mutual couplings. (Ref_1: without isolation slot, Ref_2: with isolation slot).

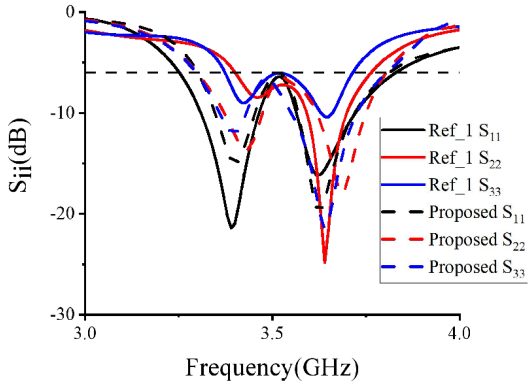

Figure 6. S-parameters of antenna elements. (Ref_1: without microstrip line, proposed: with microstrip line).

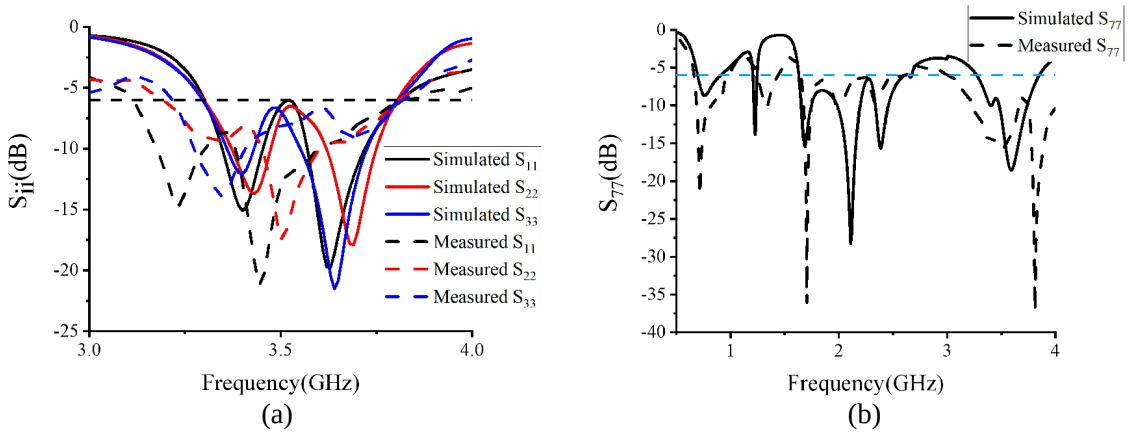

Figure 7. S-parameters of antenna elements. (a) Elements 1, 2, 3. (b) Element 7.

the system performance, we may take advantage of the existing MIMO antenna array and resort to the beamforming technique.

3. REALIZATION OF BEAMFORMING

3.1. Design Method

In order to realize the beamforming function in the transmitting mode based on the existing MIMO antenna array designed in the receiving mode, it is necessary to find the optimal distribution of excitations (ODEs) for the fixed antenna array configuration so as to achieve the highest possible gain in a desired direction. In the following, the method of maximum power transmission efficiency (MMPTE) [23–28] will be adopted to determine the ODE.

The basic working principle of MMPTE is illustrated in Fig. 10. The eight-element array under design is set as the transmitting antenna, and a test antenna is introduced as the receiving antenna and placed in the desired direction in which antenna gain must be maximized. The whole transmission system can be considered as a 9-port network and can be characterized by the scattering matrix as follows:

$$\begin{bmatrix} [b_t] \\ [b_r] \end{bmatrix} = \begin{bmatrix} [S_{tt}] & [S_{tr}] \\ [S_{rt}] & [S_{rr}] \end{bmatrix} \begin{bmatrix} [a_t] \\ [a_r] \end{bmatrix}, \tag{1}$$

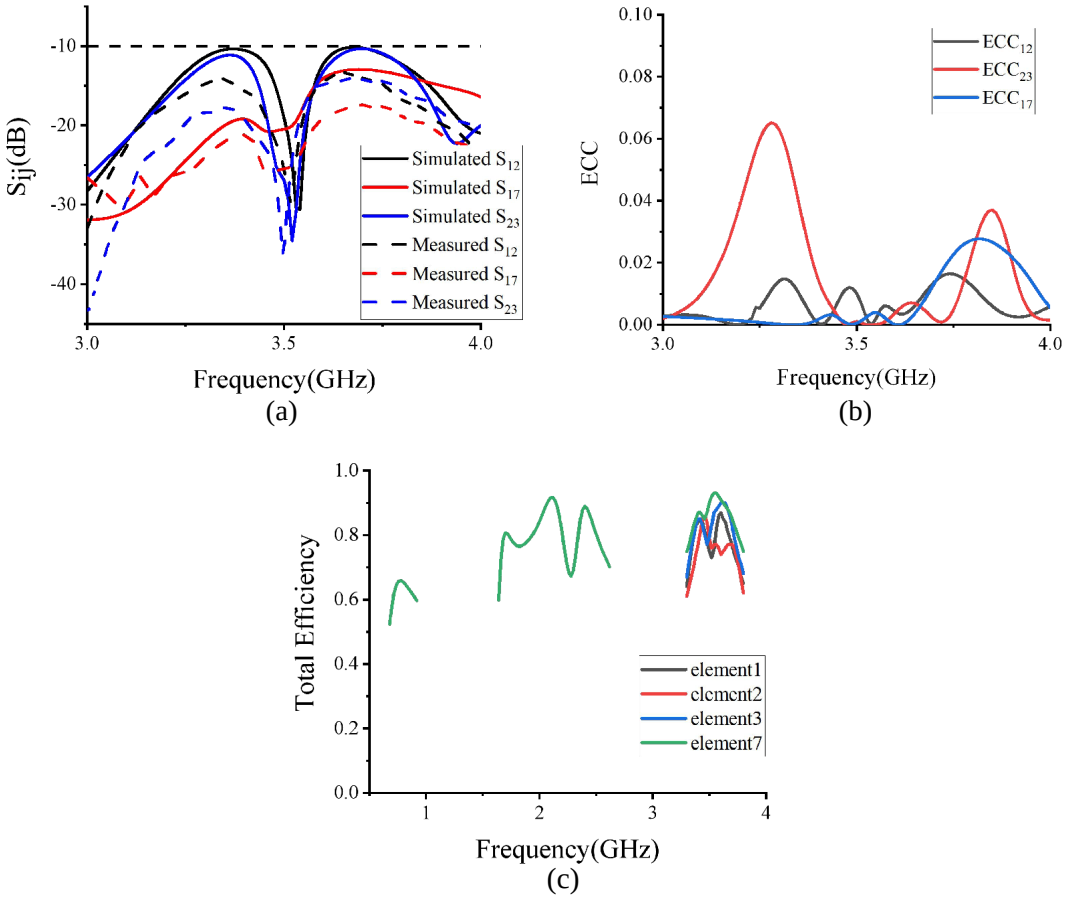

Figure 8. MIMO antenna system parameters. (a) Mutual couplings. (b) ECCs. (c) Total efficiency.

where $[a_t] = [a_1, a_2, \cdots, a_8]^T$ and $[b_t] = [b_1, b_2, \cdots, b_8]^T$ represent the normalized incident and reflected waves of the transmitting antenna array respectively; $[a_r] = [a_9]$ and $[b_r] = [b_9]$ represent the normalized incident and reflected waves of the test receiving antenna, respectively. The power transmission efficiency (PTE) of the transmission system can be expressed by [21–23]

$$T_{\text{array}} = \frac{\frac{1}{2}\left(|[b_r]|^2 - |[a_r]|^2\right)}{\frac{1}{2}\left(|[a_t]|^2 - |[b_t]|^2\right)}, \tag{2}$$

Assuming that the test antenna is matched, we have $[a_r] = 0$. If the PTE of the system reaches the maximum, the ODE for the transmitting array satisfies the following eigenvalue equation

$$[A][a_t] = T_{\text{array}}[a_t], \tag{3}$$

where $[A] = \overline{[S_{rt}]}^T[S_{rt}]$, and $[a_t]$ is the ODE for the transmitting array, which corresponds to the unique non-zero eigenvalue (the maximum PTE) and can be realized through the beamforming controller.

3.2. Digital Beamforming Controller

The in-house designed digital beamforming controller for the 8-element array has 8 channels, and each channel is composed of a single-channel TR chip AWR9621 and a power supply. The attenuation and phase shift of each channel are controlled by the micro-controller unit (MCU), which is connected to the computer via USB interface. The block diagram of the beamforming controller is shown in Fig. 11(a).

The RF signal from the input is distributed into eight channels through power splitters according to the ODE obtained from MMPTE, as illustrated in Fig. 11. To reduce the trouble in calibration, the lengths of the lines from the input to the eight TR chips are kept the same so that the phase shifts and attenuations from the input to the eight TR chips are identical. The red two-way arrows in Fig. 11

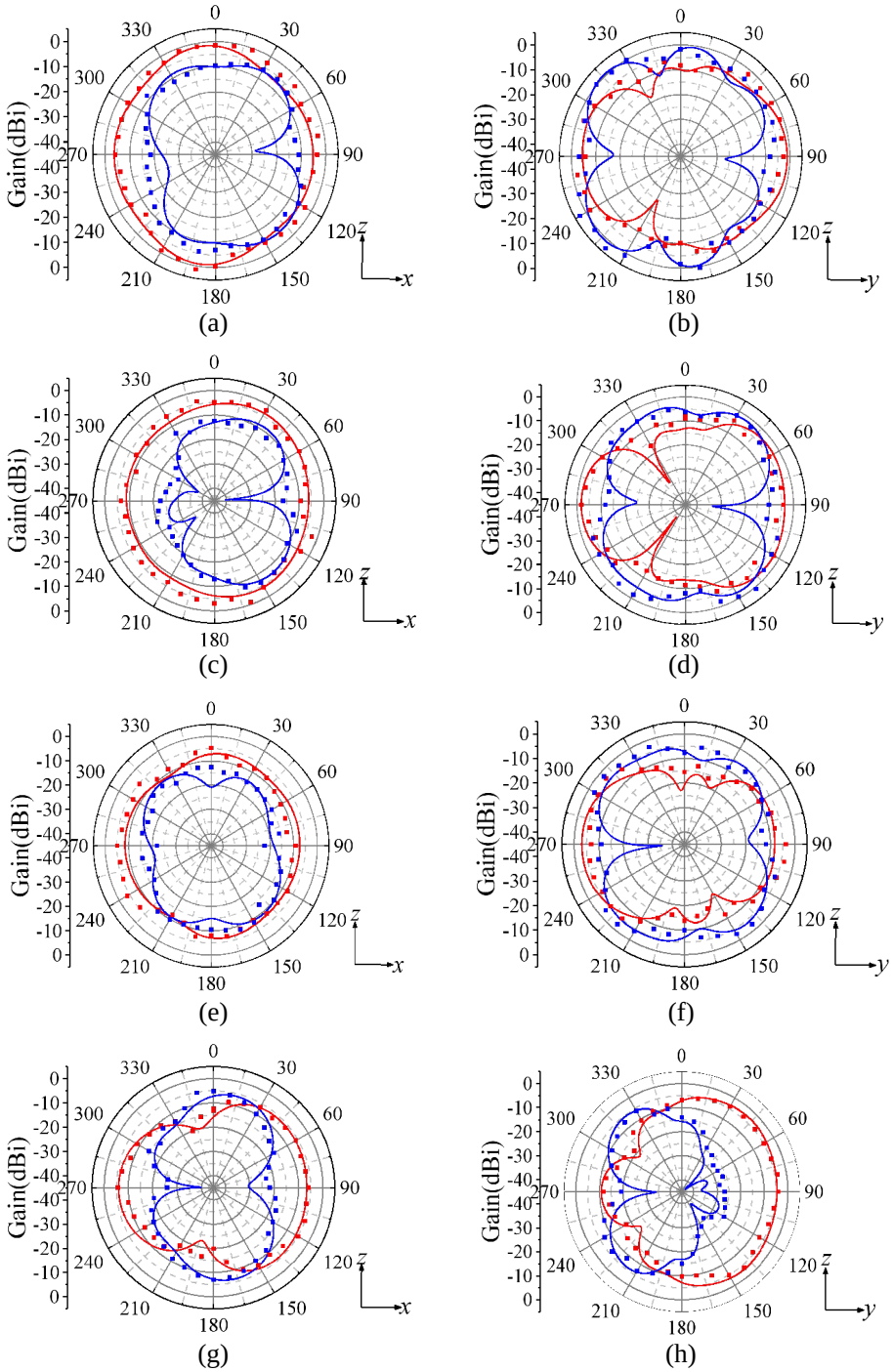

Figure 9. Measured and simulated gain patterns for antenna elements 1, 2, 3 and 7 at 3.45 GHz (— Simulated G_φ, — Simulated G_θ; - Measured G_φ, - Measured G_θ). (a) Element 1 (xz-plane). (b) Element 1 (yz-plane). (c) Element 2 (xz-plane). (d) Element 2 (yz-plane). (e) Element 3 (xz-plane). (f) Element 3 (yz-plane). (g) Element 7 (xz-plane). (h) Element 7 (yz-plane).

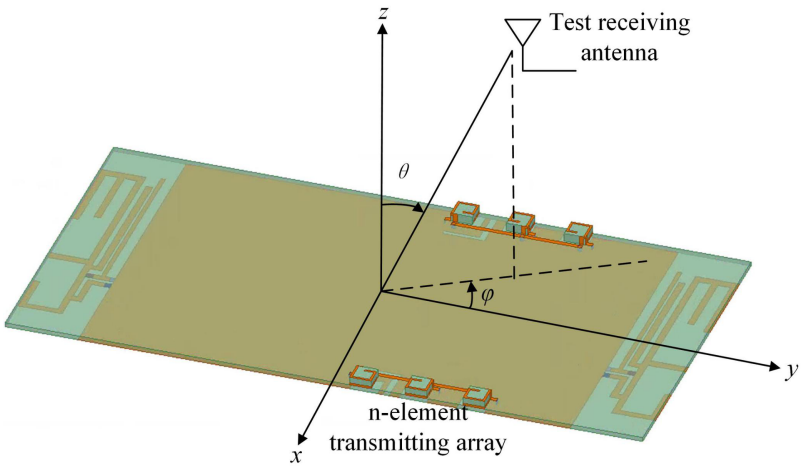

Figure 10. Power transmission system.

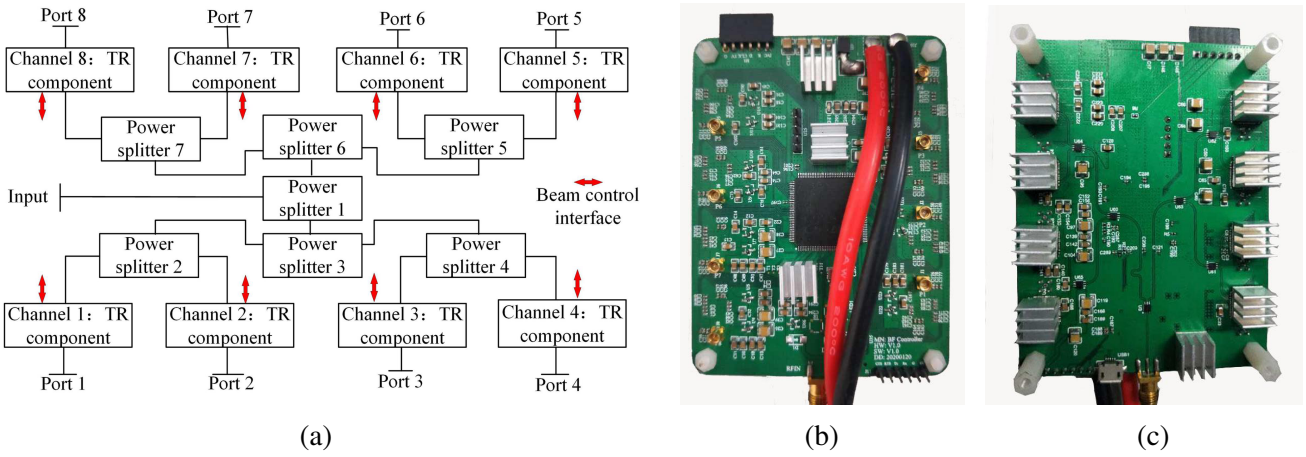

Figure 11. The block diagram and photos of digital beamforming controller. (a) Block diagram. (b) Front of photo. (c) Back of photo.

represent the beam-control interface used to connect the MCU. The attenuation and phase shift of each TR chip are controlled by MCU to realize beamforming. The photos of the beamforming controller are shown in Figs. 11(b), (c).

4. RESULTS AND ANALYSIS

Figure 12 shows photos of the 8-element antenna array. In order to compare the beamforming performance of the antenna array, we choose some elements from the eight elements to form a subarray with the rest terminated in matching loads. The beamforming performances in positive x-, y-, z-directions for different subarrays operating at 3.45 GHz are demonstrated in Table 1. One can see that the gain of the array in all directions increases as the number of array elements increases. By comparing the gain of the first module and that of the combination of the first and second modules, it can be seen that the addition of the second module can effectively improve the radiation performance. Table 2 shows the ODE calculated from MMPTE. Fig. 13 shows the 3D radiation patterns and simulated and measured 2D radiation patterns of 8-element antenna array operating at 3.45 GHz. The realized peak gains in x-, y-, and z-directions are 4.6 dBi, 4.4 dBi, and 3.7 dBi, respectively, which are significantly higher than those (less than 0 dBi) radiated from a single antenna element.

Table 1. Gain for different combinations of antenna elements at 3.45 GHz.

Antenna elements	$+x$	$+y$	$+z$
1	-5.1	-1	-1.1
1, 2, 3	-1.2	1.6	0.6
1, 2, 3, 4, 5, 6	3.8	3.7	3.7
1, 2, 3, 4, 5, 6, 7, 8	4.6	4.4	3.7

Table 2. ODE of each port of the array.

Port	$+x$	$+y$	$+z$
1	$0.28\angle -23$	$0.46\angle -3$	$0.57\angle -98$
2	$0.25\angle 78$	$0.39\angle 140$	$0.3\angle -7$
3	$0.20\angle -53$	$0.22\angle -20$	$0.22\angle -171$
4	$0.68\angle 58$	$0.21\angle -152$	$0.57\angle -105$
5	$0.37\angle 154$	$0.43\angle -1$	$0.3\angle -12$
6	$0.26\angle -11$	$0.17\angle 175$	$0.25\angle -166$
7	$0.28\angle 153$	$0.54\angle 47$	$0.18\angle -146$
8	$0.28\angle 0$	$0.19\angle 0$	$0.17\angle 0$

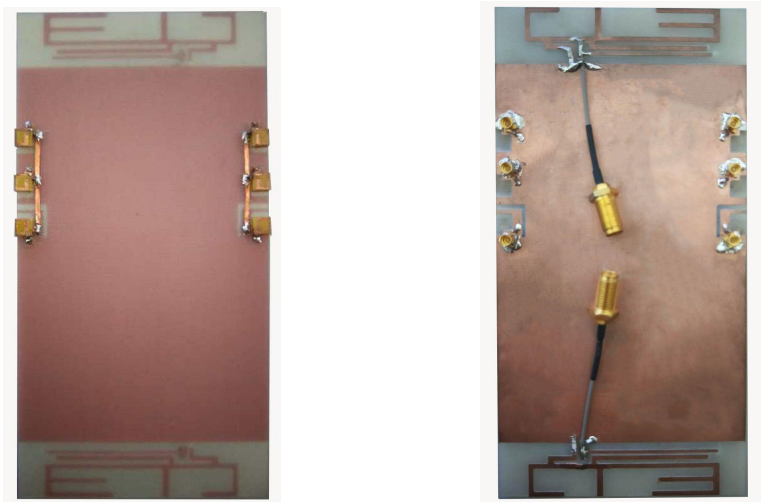

(a) (b)

Figure 12. Photos of antenna array. (a) Front. (b) Back.

5. THE INFLUENCE OF ENVIRONMENT ON THE RADIATION PERFORMANCE OF ANTENNA

The influence of the environments on the handset antenna performance is substantial and cannot be ignored in practice. For this reason, a practical handset antenna design must take the environments into account, such as the PCB, LCD, battery, and phone case. This raises a challenge for the antenna designer as the simulation of the handset antenna with all environments in place is an impossible task. Since the MMPTE is only involved with terminal parameters of the system, it can get around the

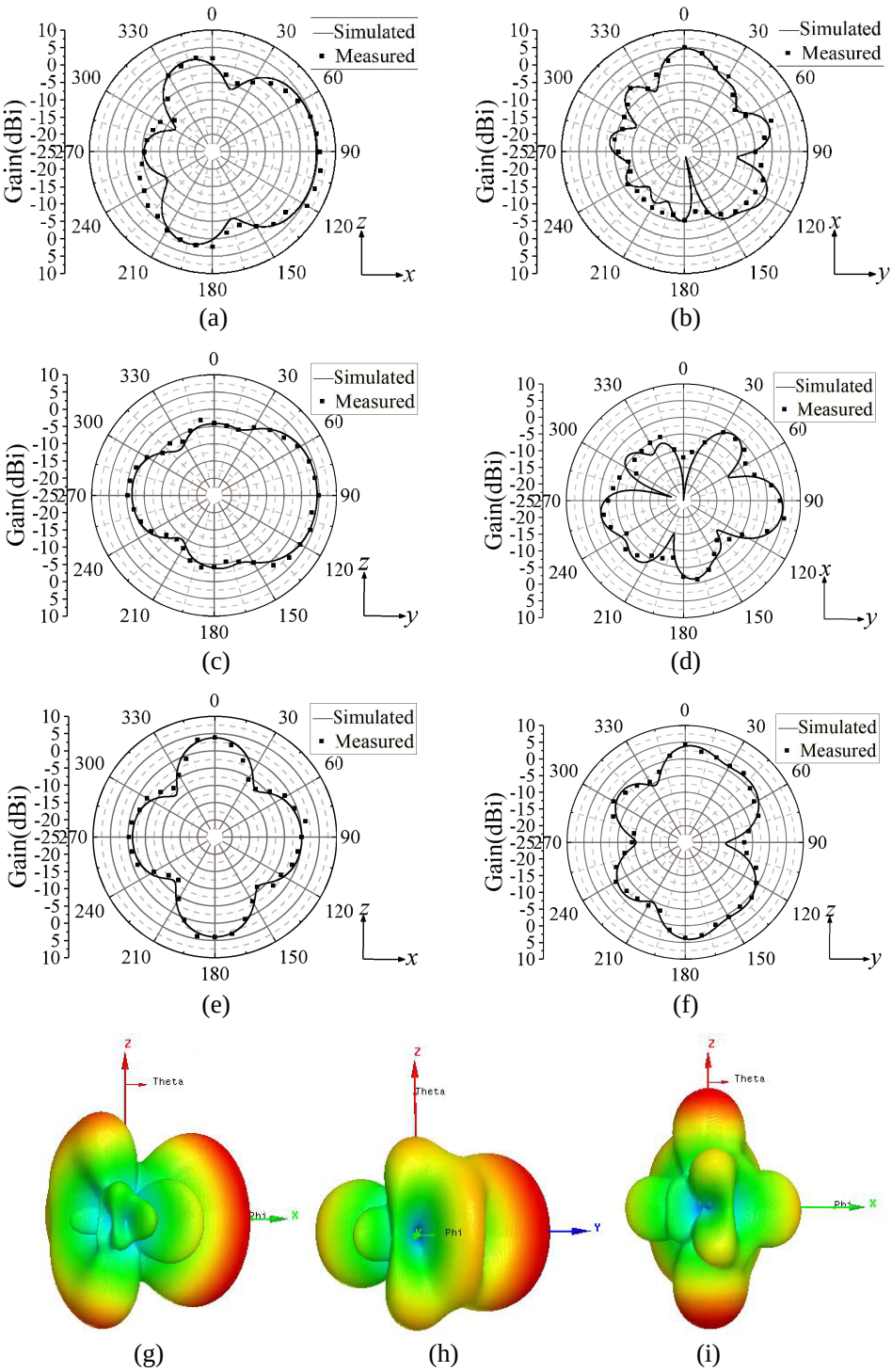

Figure 13. Measured and simulated radiation patterns of 8-element antenna array at 3.45 GHz. (a) $+x$ axis (xz-plane). (b) $+x$ axis (xy-plane). (c) $+y$ axis (yz-plane). (d) $+y$ axis (xy-plane). (e) $+z$ axis (xz-plane). (f) $+z$ axis (yz-plane). (g) $+x$ axis (3D). (h) $+y$ axis (3D). (i) $+z$ axis (3D).

challenge by resorting to measurement. To illustrate the process, we will use MMPTE to investigate the influences of the cellphone case, user's hand, and human head on the antenna radiation performances at the working frequency 3.45 GHz.

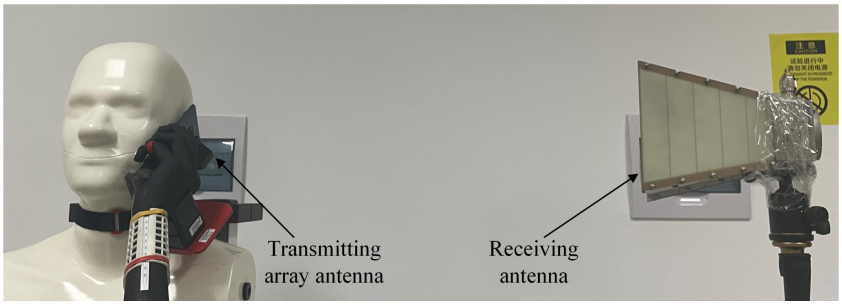

Figure 14. Measurement system with human model.

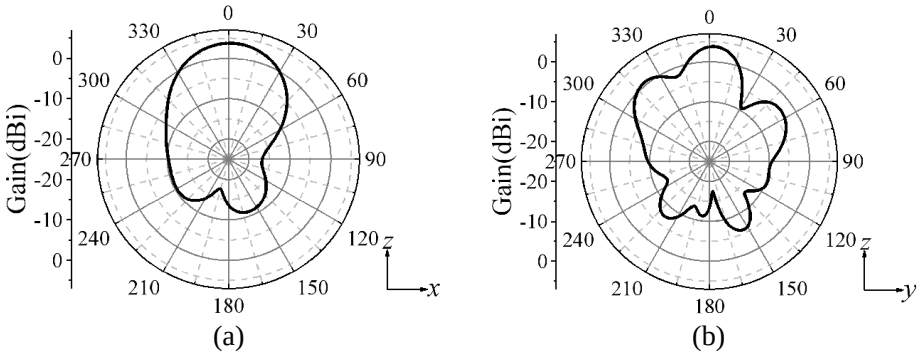

Figure 15. Radiation patterns of antenna array in airframe mode. (a) $+z$ axis (xz-plane). (b) $+z$ axis (yz-plane).

As shown in Fig. 14, a horn antenna is used as the test receiving antenna, and the 8-element antenna array placed inside the cellphone case is used as the transmitting antenna. The antenna array with the phone case is held in a hand model in the vicinity of a head model. Instead of using simulation, the scattering parameters of the transmission system are determined by the network analyzer connected to the horn antenna and the array antenna. The MMPTE is then used to calculate the ODE.

We first study the influence of the cellphone case. The cellphone case includes a screen, battery and a back cover. The screen has a dielectric constant 4.82 and loss tangent 0.0054. The back cover is plastic with dielectric constant 2.2 and loss tangent 0.005. The ODE obtained from MMPTE is listed in Table 3. Fig. 15 shows the radiation pattern of the antenna array directed to $+z$-axis with a maximum gain of 3.7 dBi. It can be seen that the antenna array still maintains a good beam performance, and

Table 3. ODE for antenna array with cellphone case.

Antenna ports	Amplitude	Phase
1	0.31	$\angle -161$
2	0.4	$\angle -21$
3	0.26	$\angle 160$
4	0.27	$\angle -164$
5	0.38	$\angle -17$
6	0.25	$\angle 165$
7	0.54	$\angle -178$
8	0.34	$\angle 0$

(a) (b)

Figure 16. (a) Simulated hand model. (b) Real hand model.

Table 4. ODE for antenna array with cellphone case and hand model.

Antenna ports	Amplitude	Phase
1	0.38	$\angle -130$
2	0.29	$\angle -27$
3	0.13	$\angle 152$
4	0.58	$\angle -109$
5	0.28	$\angle -11$
6	0.31	$\angle 126$
7	0.49	$\angle -153$
8	0.06	$\angle 0$

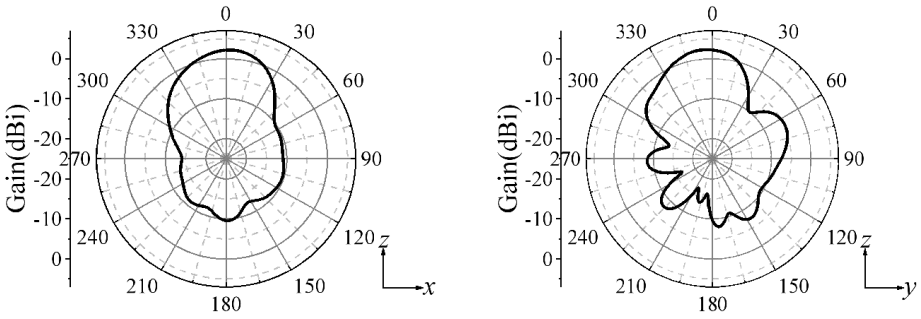

(a) (b)

Figure 17. Radiation patterns of antenna array with cellphone case and hand model. (a) $+z$ axis (xz-plane). (b) $+z$ axis (yz-plane).

its gain remains unchanged compared with that of the antenna array in free space. It is noted that the metal shield behind the LCD screen effectively blocks the radiation in $-z$ axis, thus reducing the back lobe of the beam.

Now we consider the influence of the cellphone case held by the user's hand, which corresponds to a reading position. The simulation model and a real hand model are shown in Fig. 16. Table 4 shows the ODE from MMPTE based on measured scattering parameters for the beam directed to $+z$ axis for

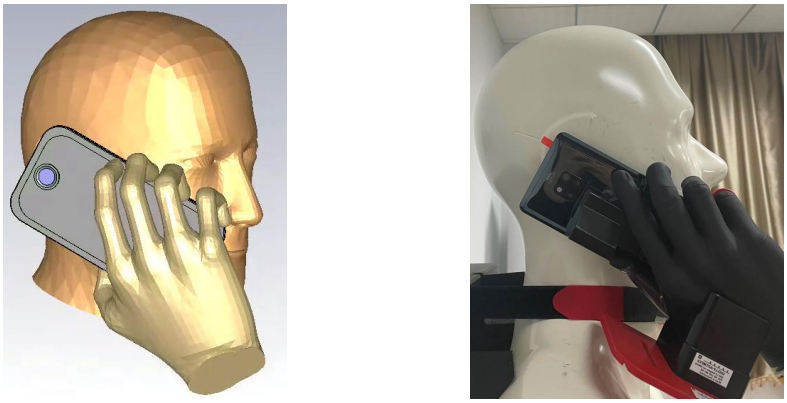

(a) (b)

Figure 18. Phone in talking position. (a) Simulation model. (b) Physical model.

Table 5. ODE of antenna array in answering call mode.

Antenna ports	Amplitude	Phase
1	0.22	$\angle 114$
2	0.65	$\angle -163$
3	0.24	$\angle 17$
4	0.43	$\angle 108$
5	0.01	$\angle 134$
6	0.29	$\angle -4$
7	0.44	$\angle 59$
8	0.07	$\angle 0$

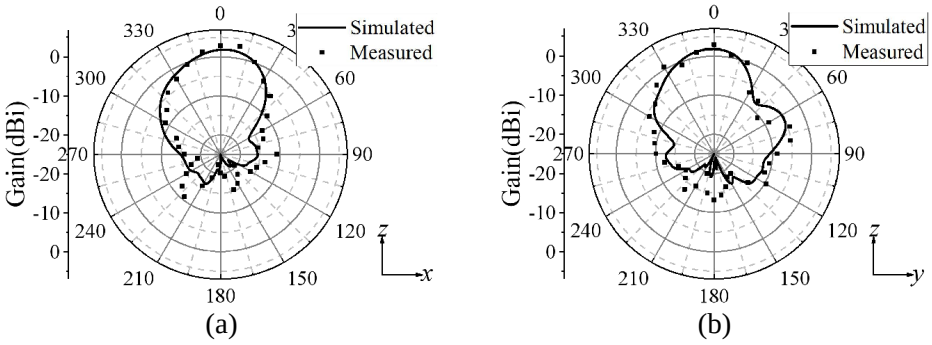

Figure 19. Radiation patterns of antenna array in talking position. (a) $+z$ axis (xz-plane). (b) $+z$ axis (yz-plane).

which the scattering parameters are obtained by measurement with the antenna array loaded with the cellphone case and the user's hand. As can be seen from the antenna radiation patterns in Fig. 17, the antenna array still maintains good beam performance with a maximum gain of 2.1 dBi. The gain is reduced by 1.6 dB compared to the antenna array in free space due to the influence of the hand model.

Finally we examine the influence of cellphone case held by the user's hand against a human head, which corresponds to a talking position. The simulation model and physical model are shown in Fig. 18.

Table 5 shows the ODE from MMPTE based on the measured scattering parameters for the beam directed to $+z$ axis in the talking position. As can be seen from Fig. 19, the antenna array still has a good beamforming performance with a maximum gain of 1.8 dBi. The simulation results are basically consistent with the measured results. The gain loss is 1.9 dB compared with that in the free space.

Table 6 shows the comparison between the proposed MIMO antenna array and other similar designs reported for mobile terminals. Only the proposed design uses different antenna elements to realize beamforming function.

Table 6. Comparison between the proposed antenna and other similar designs.

Reference	Bandwidth	Element types	MIMO order /element types	Beamforming order /element types	Environment
Proposed	2G/3G/4G/5G	2	8/2	8/2	Cellphone/Hand/Head
[3]	4G/5G	2	2/1 and 2/1	×	×
[6]	5G	2	8/2	×	Hand
[8]	LTE42/WLAN	2	8/2 and 4/1	×	Hand/Head
[9]	LTE42/43/46	3	8/2 and 6/2	×	Hand
[15]	5G	1	16/1	16/1	Hand
[20]	4G/5G	2	×	4/1	×

6. CONCLUSION

The antenna array design using different antenna elements to realize the MIMO function for receiving and beamforming function for transmitting simultaneously has not been reported before. Such an approach helps leverage the existing antenna assets in the mobile device so that the existing antenna resources can be utilized more efficiently. In this paper, an antenna array system consisting of different array modules for a handheld device has been proposed and investigated. The antenna array system is composed of two antenna modules. The first module is a 6-element antenna array operating in N78 (3.3–3.8 GHz) band for 5G, and the second module is a low profile 2-element antenna array operating in LTE/WWAN/N78 (0.7–0.91 GHz, 1.63–2.61 GHz, 3.3–3.8 GHz) bands. The first module combined with the second module forms an 8-element antenna array, which not only achieves MIMO performance for receiving in the overlapping N78 band, but also achieves beamforming for transmitting. The MIMO function is first achieved by properly designing the antenna elements and array configuration. Once the elements and configuration are fixed, the beamforming function is achieved by optimizing the feeding schemes with MMPTE so that the MIMO function is kept intact. The ODE determined by MMPTE is then realized by an in-house designed digital beamforming controller to direct the beam to a desired direction. The influences of environments, including the mobile phone case, user's hand, and human head, on the radiation performance of the antenna array are also studied. For the handset antenna surrounded by complex environment is too complicated to be handled by a computer, the ODE for the antenna array is determined by MMPTE in terms of the scattering parameters obtained from measurement, demonstrating a remarkable capability of MMPTE to solve the antenna design problem in complicated environments.

ACKNOWLEDGMENT

This work was supported by the National Natural Science Foundation of China under Grant 61971231.

REFERENCES

1. Andrews, J. G., et al., "What will 5G be?" *IEEE Journal on Selected Areas in Communications*, Vol. 32, No. 6, 1065–1082, Jun. 2014.

2. Anguera, J., A. Andújar, and C. García, "Multiband and small coplanar antenna system for wireless handheld devices," *IEEE Transactions on Antennas and Propagation*, Vol. 61, No. 7, 3782–3789, Jul. 2013.
3. Sharawi, M. S., M. Ikram, and A. Shamim, "A two concentric slot loop based connected array MIMO antenna system for 4G/5G terminals," *IEEE Transactions on Antennas and Propagation*, Vol. 65, No. 12, 6679–6686, Dec. 2017.
4. Barani, I. R. R. and K. Wong, "Integrated inverted-F and open-slot antennas in the metal-framed smartphone for 2×2 LTE LB and 4×4 LTE M/HB MIMO operations," *IEEE Transactions on Antennas and Propagation*, Vol. 66, No. 10, 5004–5012, Oct. 2018.
5. Kurvinen, J., H. Kähkönen, A. Lehtovuori, J. Ala-Laurinaho, and V. Viikari, "Co-designed mm-Wave and LTE handset antennas," *IEEE Transactions on Antennas and Propagation*, Vol. 67, No. 3, 1545–1553, Mar. 2019.
6. Li, M., et al., "Eight-port orthogonally dual-polarized antenna array for 5G smartphone applications," *IEEE Transactions on Antennas and Propagation*, Vol. 64, No. 9, 3820–3830, Sept. 2016.
7. Ren, A., Y. Liu, and C. -Y. -D. Sim, "A compact building block with two shared-aperture antennas for eight-antenna MIMO array in metal-rimmed smartphone," *IEEE Transactions on Antennas and Propagation*, Vol. 67, No. 10, 6430–6438, Oct. 2019.
8. Zou, H., et al., "Dual-functional MIMO antenna array with high isolation for 5G/WLAN applications in smartphones," *IEEE Access*, Vol. 7, 167470–167480, 2019.
9. Li, Y., C. Sim, Y. Luo, and G. Yang, "12-port 5G massive MIMO antenna array in sub-6 GHz mobile handset for LTE bands 42/43/46 applications," *IEEE Access*, Vol. 6, 344–354, 2018.
10. Ilvonen, J., R. Valkonen, J. Holopainen, and V. Viikari, "Design strategy for 4G handset antennas and a multiband hybrid antenna," *IEEE Transactions on Antennas and Propagation*, Vol. 62, No. 4, 1918–1927, Apr. 2014.
11. Ding, C. F., X. Y. Zhang, C. Xue, and C. Sim, "Novel pattern-diversity-based decoupling method and its application to multielement MIMO antenna," *IEEE Transactions on Antennas and Propagation*, Vol. 66, No. 10, 4976–4985, Oct. 2018.
12. Li, Y. R., B. Gao, X. Zhang, and K. Huang, "Beam management in millimeter-wave communications for 5G and beyond," *IEEE Access*, Vol. 8, 13282–13293, 2020.
13. Yang, B., Z. Yu, J. Lan, R. Zhang, J. Zhou, and W. Hong, "Digital beamforming-based massive MIMO transceiver for 5G millimeter-wave communications," *IEEE Transactions on Microwave Theory and Techniques*, Vol. 66, No. 7, 3403–3418, Jul. 2018.
14. Hong, W., "Solving the 5G mobile antenna puzzle: Assessing future directions for the 5G mobile antenna paradigm shift," *IEEE Microwave Magazine*, Vol. 18, No. 7, 86–102, Nov.–Dec. 2017.
15. Yu, B., K. Yang, C. Sim, and G. Yang, "A novel 28 GHz beam steering array for 5G mobile device with metallic casing application," *IEEE Transactions on Antennas and Propagation*, Vol. 66, No. 1, 462–466, Jan. 2018.
16. Helander, J., K. Zhao, Z. Ying, and D. Sjöberg, "Performance analysis of millimeter-wave phased array antennas in cellular handsets," *IEEE Antennas and Wireless Propagation Letters*, Vol. 15, 504–507, 2016.
17. Zhang, S., X. Chen, I. Syrytsin, and G. F. Pedersen, "A planar switchable 3-D-coverage phased array antenna and its user effects for 28-GHz mobile terminal applications," *IEEE Transactions on Antennas and Propagation*, Vol. 65, No. 12, 6413–6421, Dec. 2017.
18. Ojaroudiparchin, N., M. Shen, S. Zhang, and G. F. Pedersen, "A switchable 3-D-coverage-phased array antenna package for 5G mobile terminals," *IEEE Antennas and Wireless Propagation Letters*, Vol. 15, 1747–1750, 2016.
19. Li, T. and W. Geyi, "Design of MIMO beamforming antenna array for mobile handsets," *Progress In Electromagnetic Research C*, Vol. 94, 13–28, 2019.

20. Samadi Taheri, M. M., A. Abdipour, S. Zhang, and G. F. Pedersen, "Integrated millimeter-wave wideband end-fire 5G beam steerable array and low-frequency 4G LTE antenna in mobile terminals," *IEEE Transactions on Vehicular Technology*, Vol. 68, No. 4, 4042–4046, Apr. 2019.
21. Geyi, W., *Foundations of Applied Electrodynamics*, 273–275, Wiley, New York, NY, USA, 2010.
22. Geyi, W., *Foundations for Radio Frequency Engineering*, 410–420, World Scientific, 2015.
23. Geyi, W., "The method of maximum power transmission efficiency for the design of antenna arrays," *IEEE Open Journal of Antennas and Propagation*, Vol. 2, 412–430, 2021.
24. Tong, H. and W. Geyi, "Optimal design of smart antenna systems for handheld devices," *IET Microw. Antennas Propag.*, Vol. 10, No. 6, 617–623, 2016.
25. He, X., W. Geyi, and S. Wang, "A hexagonal focused array for microwave hyperthermia: Optimal design and experiment," *IEEE Antennas and Wireless Propagation Letters*, Vol. 15, 56–59, 2016.
26. Qin, Z., W. Geyi, M. Zhang, and J. Wang, "Printed eight-element MIMO system for compact and thin 5G mobile handest," *Electronic Letters*, Vol. 52, No. 6, 416–418, 2016.
27. Wan, W., W. Geyi, and S. Gao, "Optimum design of low-cost dual-mode beam-steerable arrays for customer-premises equipment applications," *IEEE Access*, Vol. 6, 16092–16098, Mar. 2018.
28. Miao, X., W. Wan, Z. Duan, and W. Geyi, "Design of dual-mode arc-shaped dipole arrays for indoor base-station applications," *IEEE Antennas and Wireless Propagation Letters*, Vol. 18, No. 4, 752–756, Apr. 2019.